GEOCHEMISTRY, MINERALOGY AND PETROLOGY • SOFIA
ГЕОХИМИЯ, МИНЕРАЛОГИЯ И ПЕТРОЛОГИЯ • СОФИЯ
2009, **47**, 11-30.

Moraine-hosted Cu-Bi-mineralization from the Modi-Khola valley, southwestern flank of Annapurna-III, Central Himalaya

Kalin Kouzmanov, Ivan K. Bonev, Rossitsa D. Vassileva

Abstract. The Cu-Bi-Ag-Te mineralization found in moraine blocks in the central part of the Modi-Khola valley, on the southwestern flank of Annapurna-III in central Nepal can be defined as a new type post-collisional hydrothermal system in the High Himalaya, related to a Miocene magmatic event of leucocratic granite intrusions or equigranular pegmatite bodies. The mineral assemblage consists dominantly of chalcopyrite and pyrite, with variable amounts of Bi-Ag sulphides, sulphosalts and tellurides (bismuthinite, tetradymite, hessite, aikinite-bismuthinite derivates). Ilmenite, magnetite, cubanite, garnet, rutile, chlorite and quartz complete the mineral assemblage. Common complex intergrowth textures, involving aikinte, hessite and tetradymite in highly variable proportions and forming equilibrium assemblages, resulted from segregation and crystallization of "droplets" of Ag-Bi-Te-(S) "melts" from the hydrothermal fluids at temperatures above the melting point of bismuth. Thus, the mineralization can be considered as mesothermal ore formation, most probably resulting from a magmatic-hydrothermal system that was active during the mid-Miocene in the Annapurna Himal.

Keywords: Cu-Bi-Ag-Te mineralization, Bi-minerals, tellurides, Modi-Khola, Annapurna, Greater Himalaya

Addresses: K. Kouzmanov - Department of Mineralogy, University of Geneva, Rue des Maraîchers 13, 1205 Geneva, Switzerland; E-mail: kalin.kouzmanov@unige.ch; R. Vassileva - Geological Institute, Bulgarian Academy of Sciences, 1113 Sofia, Bulgaria

Калин Кузманов, Иван К. Бонев, Росица Д. Василева. Cu-Bi-минерализация в морени от долината на река Моди-Кхола, в югозападното подножие на Анапурна-III, Централни Хималаи

Абстракт. Cu-Bi-Ag-Te минерализация, намираща се в моренните блокове от централната част на долината на река Моди-Кхола, от югозападната страна на Анапурна-III в централен Непал, може да се определи като нов тип пост-колизионна хидротермална система във Високите Хималаи, свързана с внедряването на миоценски левкократни гранити или равномерно зърнести пегматитови тела. Минералната асоциация е изградена основно от халкопирит и пирит, с различно количество Bi-Ag сулфиди, сулфосоли и телуриди (бисмутинит, тетрадимит, хесит, айкинит-бисмутинитови деривати). Илменит, магнетит, кубанит, гранат, рутил, хлорит и кварц допълват минералното разнообразие. Често срещани са сложни текстурни прораствания, включващи айкинит, хесит и тетрадимит в широко вариращи пропорции, формиращи равновесни асоциации и образувани в резултат на сегрегация и кристализация на «капчици» Ag-Bi-Te-(S) «топилка» в хидротермалните флуиди при температури надвишаващи температурата на топене на бисмута. По този начин, минерализацията може да се счита за мезотермална рудна формация, образувана вероятно от магматично-хидротермална система, която е била активна през средния Миоцен в района на Анапурна, Високи Хималаи.

Introduction

The formation of the Himalayan range – the highest mountain system in the world, is a result of the Eocene (~50 Ma) collision between the Indian and Asian continents and subsequent convergence, deformation and uplift, which continue to present day. The geology of the orogen results from complex processes involving sedimentation, metamorphism, granitization, magmatism and intensive tectonic movements over an area extending for thousands of kilometers along strike. The orogen is built on a complex tectonic collage created by accretion of several terranes onto the southern margin of the Asian continent since the early Paleozoic (Allègre et al. 1984). Tectonic activity, metamorphism and magmatism in central Nepal occupying the central part of the orogen have been extensively studied in the last decades (Bordet et al. 1971; Colchen et al. 1986; Garzanti 1999; Godin 2003; Godin et al. 2006).

High heat flows, resulting from the collisional orogeny and associated crustal thickening, translithospheric shearing, and lithospheric mantle thinning, are regarded as the main causes for hydrothermal mineralization in the orogenic belts (Seltmann & Faragher 1994). However, the metallogenesis of collisional orogens is still poorly understood, due to the lack of systematic studies on the genetic links between collisional processes and ore formation in collisional orogenic belts. Recently, Hou & Cook (2009) summarized the metallogenic features of the Tibetan collisional orogen, hosting a variety of ore-forming systems: (1) porphyry Cu–Mo systems related to high-K adakitic stocks derived from the newly-formed thickened mafic lower-crust; (2) vein-type Sb–Au ore systems controlled by the South Tibetan detachment system (STDs) and the metamorphic core complex or thermal dome intruded by leucogranite intrusions; (3) hydrothermal Pb–Zn–Ag ore systems controlled by the intersections of N–S-striking normal faults with E–W-trending thrust faults; and (4) spring-type Cs–Au ore systems related to geothermal activity driven by partial melting of the upper crust. Metallogenic studies in the central part of the Himalayan range in central Nepal are scarce, compared to the better studied Tibetan eastern part of the orogen (Hou & Cook 2009 and references therein), but the similar geological setting is a good prerequisite to expect similar ore mineralization styles in the area.

In this contribution, we studied moraine-hosted Cu-Bi mineralization, exposed in the upper part of the Modi-Khola valley, close to the Annapurna Sanctuary, central Nepal. The main difficulty to work on moraine-hosted mineralization comes from the missing information about the direct host rock such as alteration styles, geometry and morphology of the mineralized structures, extension of the hydrothermal system. Based on paragenetic sequence and mineral chemistry we discuss the possible origin of the studied mineralization.

Geological setting and provenance of the samples studied

Annapurna Sanctuary is located in central Nepal and represents a large glacier circus bordered by the mountain range of Hiunchuli, Annapurna South, Annapurna-I and III, and Machapuchare peaks. The narrow section of the Modi Khola valley provides the only access to the Annapurna Sanctuary. The samples under investigation belong to an area in the western banks of the Modi-Khola River, on the southwestern flank of the Annapurna-III peak (Fig. 1). The moraines which are constantly piled there comprise rock fragments belonging to the upper in relief succession. The river crosscuts meridionally the mountain range, forming deep section through the sequence. The range of Annapurna peaks follows the general E-W orientation of the tectonic

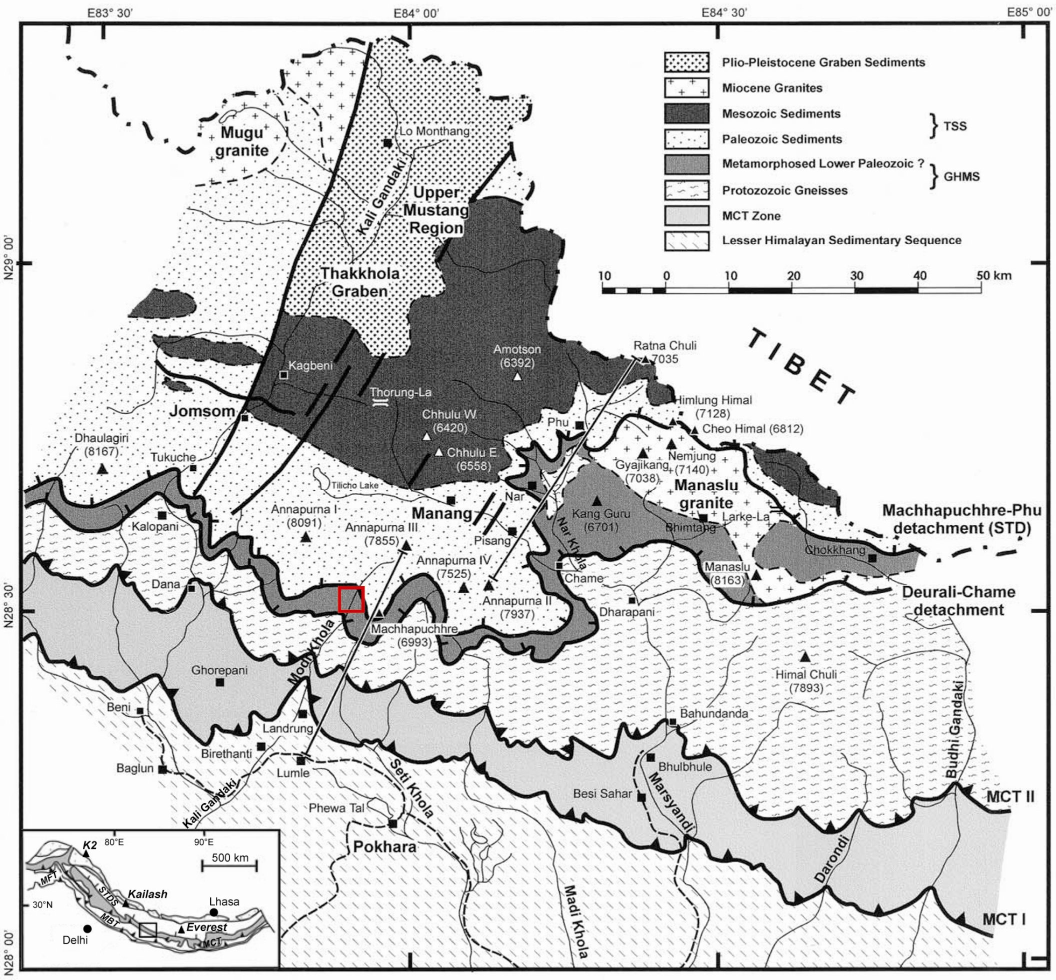

Fig.1. Regional geological map, modified after Searle & Godin (2003). Inset shows the main units within the Himalayan orogen (after Godin et al. 2006): Greater Himalayan sequence in grey; important structures noted are Main Frontal thrust (MFT), Main Boundary Thrust (MBT), Main Central Thrust (MCT), and South Tibetan detachment system (STDS). Solid red rectangle refers to the studied area

boundaries in the Himalayan orogen (Fig. 1).

The Modi-Khola valley cuts through three laterally continuous, fault-separated tectono-stratigraphic rock assemblages of the central Himalayan orogen (Fig. 2; Gansser 1964; Bordet et al. 1971; Colchen et al. 1986; Garzanti 1999; Yin & Harrison 2000; Godin 2003); from north to south – Tethyan sediments, the Greater Himalayan metamorphic sequence and the Lesser Himalaya sediments. Two Miocene north-dipping tectonic faults with opposite sense of shearing separate the three major tectonostratigraphic units. The structurally lower fault is termed the Main Central Thrust (MCT), and the structurally higher is called the South Tibetan Detachment system (STD - Godin et al. 2001; Godin 2003; Searle et al. 2003).

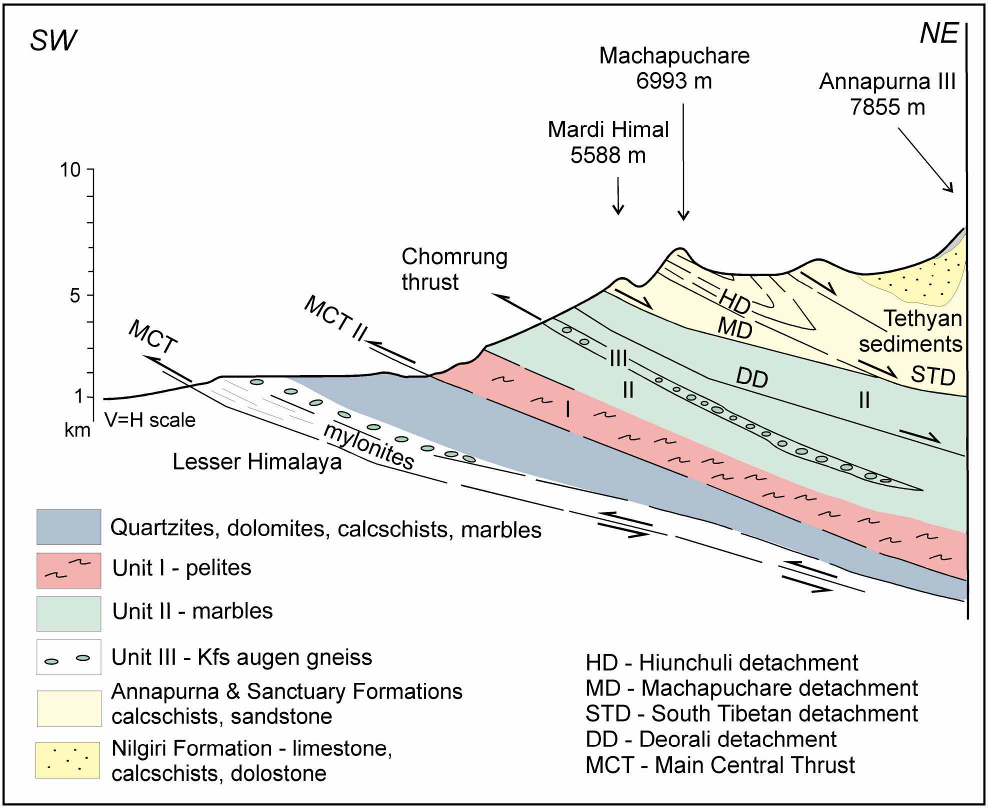

Fig. 2. Geological cross-section along the Modi-Khola valley, modified after Hodges et al. (1996) and Searle & Godin (2003). I, II, III refer to the informal units of the Greater Himalayan metamorphic sequence (see text for details)

The *Tethyan sedimentary sequence*, presenting the northernmost lithotectonic unit consists of continuous sedimentary succession of Neoproterozoic to Eocene rocks being nearly 10-km thick (Colchen et al. 1986; Murphy & Yin 2003). It is bound to the north by the Indus–Yarlung suture zone, presenting the former subduction zone between the Indian and the Asian plates and extends southwards to the South Tibetan Detachment System. The Tethyan sediments in the Annapurna area consist of the Annapurna and Sanctuary Formations with Cambrian-Ordovician age (Godin 2003).

The *Greater Himalayan metamorphic sequence* comprises the exhumed metamorphic core of the Himalayan orogen, bounded by MCT and STD (Godin et al. 2006). Composed of kyanite and sillimanite grade gneisses the rocks of the unit are also intruded by Miocene leucogranites (Inger & Harris 1993). The Greater Himalayan sequence in central Nepal is informally subdivided into three units (Le Fort 1975, 1981; Colchen et al. 1986; Guillot et al. 1995; Searle & Godin 2003): (1) the structurally lowest Unit I, consists of schists and gneisses formed by metamorphism of sedimentary succession dominated by mudstones and interbedded minor sandstones; (2) Unit II is dominantly calc-silicate and consists of marbles and layered calc-silicate shists and calc-silicate gneisses. This formation sits structurally above Unit I; (3) K-feldspar augen gneisses known as granitic Unit III intrude near the structural top of Unit II.

The southernmost tectonostratigraphic unit is presented by the *Lesser Himalayan sedimentary sequence*, compiled by a succession of Precambrian to Mesozoic unmetamorphozed sediments to low-grade metamorphic rocks (Stöcklin 1980; Parrish & Hodges 1996; Dhital et al. 2002).

The MCT is the structure that bounds the base of the Greater Himalayan series. It was mapped based on stratigraphic, lithological, isotopic or geochronological criteria (Le Fort 1975; Colchen et al. 1986; Pêcher 1989). Thrusting the higher-grade Greater Himalayan metasedimentary rocks onto the lower-grade Lesser Himalayan metasedimentary rocks, the MCT is described as a complex high-strain shear zone affecting both the upper part of the Lesser Himalayan sediments and the lower section of the Greater Himalayan metamorphic sequence.

The STD marks the top of the Greater Himalayan series, and consists of series of north-dipping normal faults (Searle et al. 2003). It places less-metamorphosed Tethyan metasedimentary rocks series onto strongly-metamorphosed Greater Himalayan series metasedimentary rocks.

Felsic magmatism involving recycling of continental material is known in the Lesser and Greater Himalayan zone (Inger & Harris 1993; Harrison et al. 1995). The heat sources of the Tertiary metamorphism and anatexis in the Annapurna – Manaslu region are described by England et al. (1992) as crustal thickening and slip on the MCT. In the succession of the Greater Himalayan sequence, the manifestation of such processes can be seen in the Unit III gneisses and in the Oligocene-Miocene leucogranite belt (Le Fort & Raï, 1999). Hodges et al. (1996) determined the age of leucogranite intrusion and Unit II in the valley of Modi-Khola and Annapurna Sanctuary as early-Miocene. Although the leucogranites from the high Himalayan zone are frequently found to form some of the highest peaks, they are structurally in the footwall of the STD and never crosscut the fault plane to intrude in the overlying Tethyan sediments (Searle et al. 2008). The U-Th-Pb dating of these leucogranites from Zanskar in the west to Bhutan in the east show ages in the range ~24 to ~12, mostly ~22 to ~19 Ma (Searle & Godin 2003 and references therein). The Manaslu granites, which intrude the STD plane and reach up the Triassic sediments in the Tethyan sequence (Guillot et al. 1995) are an exception. Harrison et al. (1999) defined two pulses of magmatism at 22.9 ± 0.6 Ma and 19.3 ± 0.3 Ma by Pb/Th ion microprobe dating of monazites from the Manaslu leucogranite. The Manaslu leucogranite can be regarded as a potential magmatic source for the studied mineralization (see below).

In the middle part of the section along the Modi-Khola valley pegmatites are widespread within the calc-silicate rock sequence. Two genetically different pegmatite types can be distinguished – early *type-I* (fine- to equigranular, showing shistosity parallel to the calc-silicate layers) and *type-II* (coarse-grained, clearly cross-cutting the *type-I* pegmatites and Unit-II lithologies). Pyrite altered to limonite can be observed in the central part of the pegmatite bodies (Vassileva & Bonev 2008).

To our knowledge, there is no indication for other hydrothermal activity in the area except for the hot springs along the Modi-Khola valley. Craw (1990) suggested that the locally high temperature of springs presumably reflect advective movement of deep, hot fluids to shallow levels along highly faulted plumbing systems and hence the presence of warm thermal waters in the Annapurna Himal does not indicate fluid convection in high near-surface conductive heat flow.

Samples and analytical techniques

Three texturally different types of ore samples have been collected by the second author during an expedition in central Nepal in 1987. Lately, they were prepared as polished mounts in epoxy raisin (Fig. 3). Type-1 corresponds to hydrothermal breccia affecting strongly silicified marbles (Fig. 3a). The breccia matrix

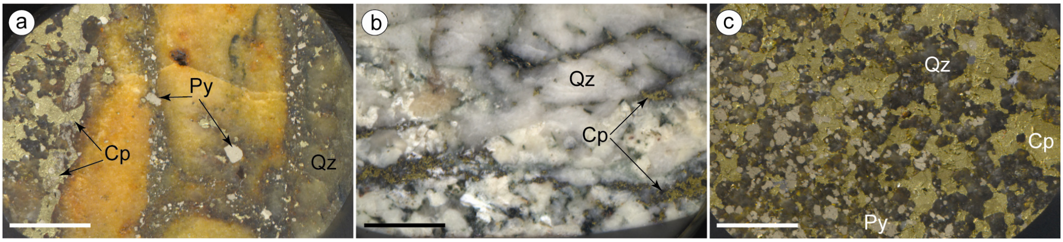

Fig. 3. Textures: a) Type-1 – hydrothermal breccia in strongly silicified marbles; b) Type-2 – quartz-chalcopyrite veinlets and disseminations hosted by a leucocratic granitic rock; c) Type-3 – massive aggregate of fine-grained chalcopyrite, pyrite and quartz. Scale bar corresponds to 5 mm. *Abbreviations:* (Cp) chalcopyrite; (Py) pyrite; (Qz) quartz

consists of fine-grained quartz, pyrite and chalcopyrite. Type-2 consists of quartz-chalcopyrite veinlets and disseminations hosted by a leucocratic granitic rock (Fig. 3b). Type-3 is a massive aggregate of fine-grained chalcopyrite, pyrite and quartz (Fig. 3c). The origin of the host rock for type-3 mineralization was not possible to be determined, but since the mineral composition of type-3 is similar to type-1 (see below) it can be assumed as more massive parts of the hydrothermal breccia of type-1 mineralization.

Systematic reflected light microscopy was performed prior to electron microscopy (back-scattered electron (BSE) imaging and EDS analyses). Electron microprobe analyses (EMPA) and X-ray elemental mapping were carried out using the Jeol JXA 8200 Superprobe WD/ED combined microanalyzer at the University of Lausanne. Operating conditions were accelerating voltage of 15 kV, beam current of 20 nA, and beam diameter of 1 µm. Standards and radiations used were as follows: FeS_2 (Fe-$K\alpha$, S-$K\alpha$), GaAs (As-$L\alpha$), Sb_2S_3 (Sb-$L\alpha$), Cu metal (Cu-$K\alpha$), PbS (Pb-$M\alpha$, S- $K\alpha$), Te metal (Te-$L\alpha$), Bi_2Se_3 (Bi-$M\alpha$, Se-$L\alpha$), Ag metal (Ag-$L\alpha$). Counting times of 20 s on peak and 10 s on background on both sides of the peak were used for all elements. Overlap and matrix corrections were carried out following the established protocol and software in the laboratory.

Mineral paragenesis

The paragenetic sequence observed in the studied samples is summarized in Fig. 4. Two stages of mineralization are defined based on the two generations of pyrite observed. In type-1 samples an early generation of pyrite, intergrown with marcasite, is replaced by ilmenite and chalcopyrite (Fig. 5a). No other

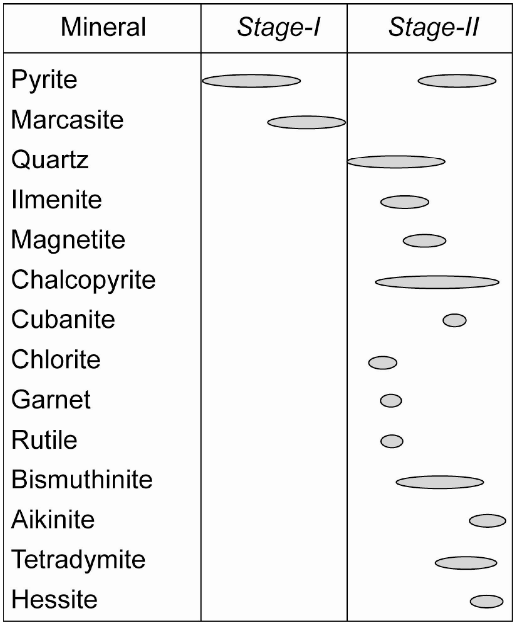

Fig. 4. Paragenetic sequence of the studied samples

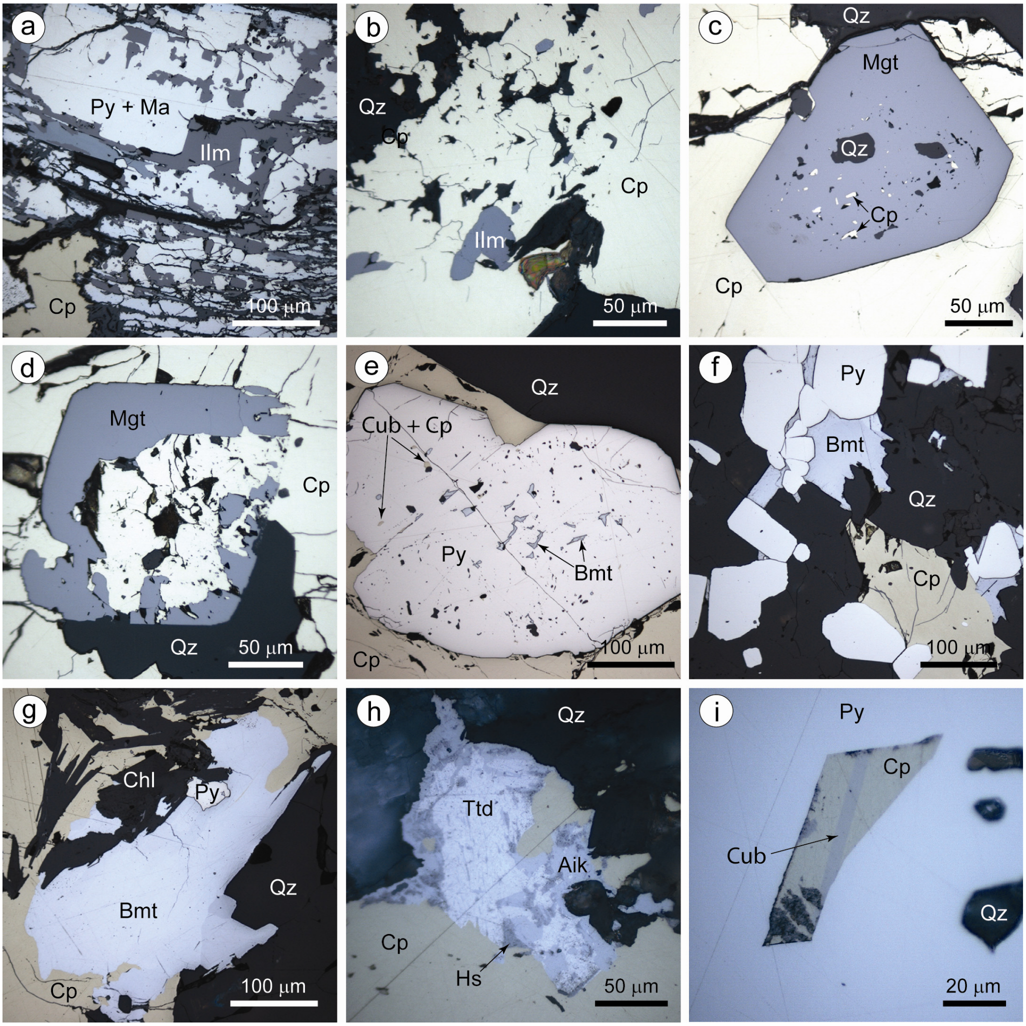

Fig. 5. Reflected light microphotographs: a) Pyrite and marcasite from stage-I replaced by ilmenite and chalcopyrite from stage-II; b) Idiomorphic ilmenite inclusions intergrown with chlorite in chalcopyrite; c) Idiomorphic magnetite crystal with chalcopyrite, pyrite and quartz inclusions in massive chalcopyrite; d) Magnetite, partially replaced by chalcopyrite and quartz; e) Pyrite with abundant bismuthinite, chalcopyrite and cubanite inclusions, associated with chalcopyrite and quartz; f) Bismuthinite intergrown with pyrite, chalcopyrite and quartz; g) Bismuthinite intergrown with chlorite, pyrite, chalcopyrite and quartz; h) Complex tetradymite-hessite-aikinite intergrowth in chalcopyrite; i) Cubanite-chalcopyrite inclusion in pyrite. *Abbreviations:* (Aik) aikinite; (Bmt) bismuthinite; (Chl) chlorite; (Cp) chalcopyrite; (Cub) cubanite; (Hs) hessite; (Ilm) ilmenite; (Ma) marcasite; (Mgt) magnetite; (Py) pyrite; (Ttd) tetradymite; (Qz) quartz

opaque mineral is paragenetically related to them. Most probably, the strong silicification of the host marble took place also during stage-I. The mineral assemblage common to type-1, 2 and 3 samples and forming the stage-II consists of pyrite-2, quartz, ilmenite, magnetite, chalcopyrite and cubanite. In addition, bismuthinite is observed in type-1 and 3 samples, while complex intergrowth textures involving aikinite, tetradymite and hessite, as well as single tetradymite crystals are typical for type-2 samples. Oxides – ilmenite and magnetite, predominantly as idiomorphic crystals, are associated with chalcopyrite (Figs. 5b-d). Magnetite is sometimes partially replaced by chalcopyrite. Pyrite-2 forms idiomorphic crystals, containing numerous single or composite inclusions of chalcopyrite, bismuthinite and cubanite (Figs. 5e and 5i). Bismuthinite also occurs as large aggregates associated with pyrite, chalcopyrite and quartz (Figs. 5f-g and 6a). In one sample of type-3 mineralization, bismuthinite is intergrown with quartz, zoned garnet, rutile and chlorite (Fig. 6b). Chlorite is a widespread mineral within the assemblage, often intergrown with chalcopyrite and bismuthinite (Fig. 5g). When complex intergrowths of tetradymite, aikinite and hessite are observed in quartz-chalcopyrite veins and disseminations in type-2 mineralization, bismuthinite is absent (Fig. 5h). The proportion between the three mineral phases changes significantly in the different structures, suggesting complex intergrowth mechanism of formation, instead of breaking-down of a mineral phase with intermediate composition (Figs. 5h, 6d-f, 7). Tetradymite also occurs as single long-prismatic inclusions in chalcopyrite (Fig. 6c).

Mineral compositions

Compositional data for major and trace elements in the main minerals, forming the studied assemblage, based on electron microprobe analysis, are reported in Tables 1-3.

Pyrite and *marcasite (FeS_2)* from stage-I are completely depleted in trace elements, within the limits of detection of the microprobe, using the given analytical conditions. Pyrite from stage-II does not contain significant trace elements either: only Cu, As, Ag and Te have been detected sporadically (Table 1), but usually these elements are in concentrations below the detection limit too.

Chalcopyrite ($CuFeS_2$) is also depleted in trace elements (Table 1). Tellurium is the only element systematically present in concentrations of few hundreds of ppm. The mineral is generally stoichiometric, showing just slight Fe excess (Fe/Cu varies from 1.01 to 1.04). No variation in its chemistry has been noted as a function of the mineral association.

Cubanite ($CuFe_2S_3$) is present only as inclusions in pyrite, and often intergrown with chalcopyrite. It has near stoichiometric composition, with slight Cu excess over Fe (Fe/Cu ratio 1.94-1.97). No trace elements have been detected, except 500 ppm Te in a single analysis (Table 1).

Bismuthinite (Bi_2S_3) from both type-I and type-III mineralizations has very similar composition (Table 2; Fig. 8). Copper, antimony and lead are constantly present in concentrations of 0.67-1.55 wt.%, 0.22-0.60 wt.%, and 2.01-4.52 wt.%, respectively. Iron, selenium and tellurium were also detected, usually in concentrations of few hundreds of ppm. Silver was sporadically detected (in 7 out of 40 analyses) and its concentrations vary between 700 and 900 ppm, exceptionally reaches 1300 ppm. No significant correlation has been observed between major and trace elements, or between different trace elements.

Tetradymite (Bi_2Te_2S) occurring as individual inclusions in chalcopyrite and as part of the complex intergrowth textures with hessite and aikinite differs in minor element concentrations. The chalcopyrite-hosted tetradymite inclusions are enriched in Pb (up to 11.54 wt.%; Fig. 9a), compared to the tetradymite from the complex intergrowths (up to 1.44 wt.% Pb, usually <1wt.% Pb). The other trace elements have almost constant concentrations in both types of tetradymite; Fe (usually <1wt.%), Cu (0.3-1.7 wt.%), Se (~1wt.%). Silver is also present, generally <1 wt.%, but in some cases its concentration can reach up to 17 wt.% (Table 3). Iron and copper in both types of tetradymite show strong positive correlation (Fig. 9b), which differs from the 1:1 line, thus excluding possible

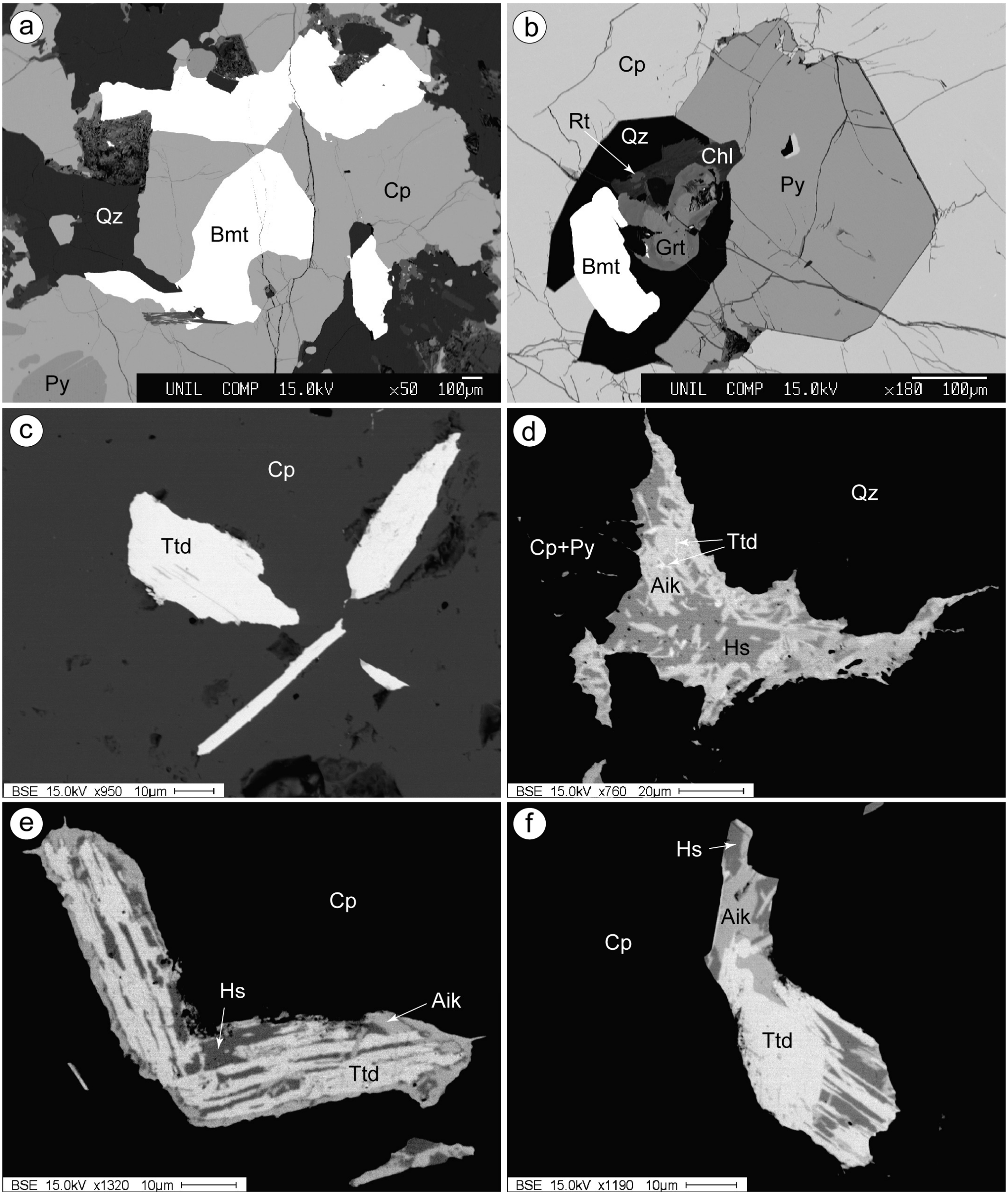

Fig. 6. Back-scattered electron (BSE) images: a) Large bismuthinite crystals in chalcopyrite; b) Bismuthinite intergrown with quartz, garnet, chlorite and rutile, in association with pyrite and chalcopyrite; c) Prismatic single crystals of tetradymite as inclusions in chalcopyrite; d-f) Complex tetradymite-hessite-aikinite intergrowth textures; note the highly variable proportion of the three phases. *Abbreviations:* (Aik) aikinite; (Bmt) bismuthinite; (Chl) chlorite; (Cp) chalcopyrite; (Cub) cubanite, (Grt) garnet; (Hs) hessite; (Py) pyrite; (Rt) rutile; (Ttd) tetradymite; (Qz) quartz

Table 1: *Electron microprobe analyses of pyrite, chalcopyrite and cubanite*

		Analysis (wt. %)							Atomic %						
No	Label	S	Fe	Cu	As	Ag	Te	Total	S	Fe	Cu	As	Ag	Te	
Pyrite															*S/Fe*
1	AN-11_14	53.00	46.25	n.d.	0.07	n.d.	0.09	99.42	66.58	33.36		0.04		0.03	2.00
2	AN-11_15	53.17	46.62	n.d.	n.d.	0.03	n.d.	99.81	66.49	33.48		0.02	0.01		1.99
3	AN-60_2	54.15	46.01	0.07	n.d.	n.d.	n.d.	100.23	67.18	32.78	0.04				2.05
4	AN-40_1	53.40	46.36	n.d.	n.d.	n.d.	n.d.	99.76	66.74	33.26					2.01
Chalcopyrite															*Fe/Cu*
1	AN-11_C	34.55	30.18	33.94	n.d.	n.d.	0.04	98.71	50.06	25.11	24.82			0.01	1.01
2	AN-11_M	34.91	30.19	33.86	n.d.	n.d.	n.d.	98.96	50.35	25.01	24.64				1.01
3	AN-35A_A	34.60	29.98	33.75	n.d.	n.d.	0.08	98.40	50.24	25.00	24.73			0.03	1.01
4	AN-35A2_B	34.56	29.75	33.88	n.d.	n.d.	n.d.	98.20	50.28	24.85	24.87				1.00
5	AN-40-1_B	34.53	30.13	33.99	n.d.	n.d.	n.d.	98.64	50.06	25.08	24.86				1.01
6	AN-40-1_A	34.80	29.90	34.56	n.d.	n.d.	0.04	99.30	50.13	24.73	25.12			0.02	0.98
7	AN-11_6	34.76	30.20	33.14	n.d.	n.d.	0.06	98.15	50.50	25.19	24.30			0.02	1.04
8	AN-11_7	35.70	30.27	33.11	n.d.	0.04	0.10	99.22	51.12	24.89	23.93		0.02	0.04	1.04
9	AN-60_2	35.08	30.12	33.94	0.05	n.d.	n.d.	99.20	50.46	24.87	24.64	0.03			1.01
Cubanite															*Fe/Cu*
1	AN-40-1_E	35.41	40.23	23.56	n.d.	n.d.	0.05	99.25	50.29	32.81	16.88			0.02	1.94
2	AN-40-1_E	35.45	40.56	23.39	n.d.	n.d.	n.d.	99.40	50.25	33.01	16.73				1.97

n.d. - below limit of detection; LOD - Cu (0.06). As (0.04). Ag (0.03). Te (0.04)

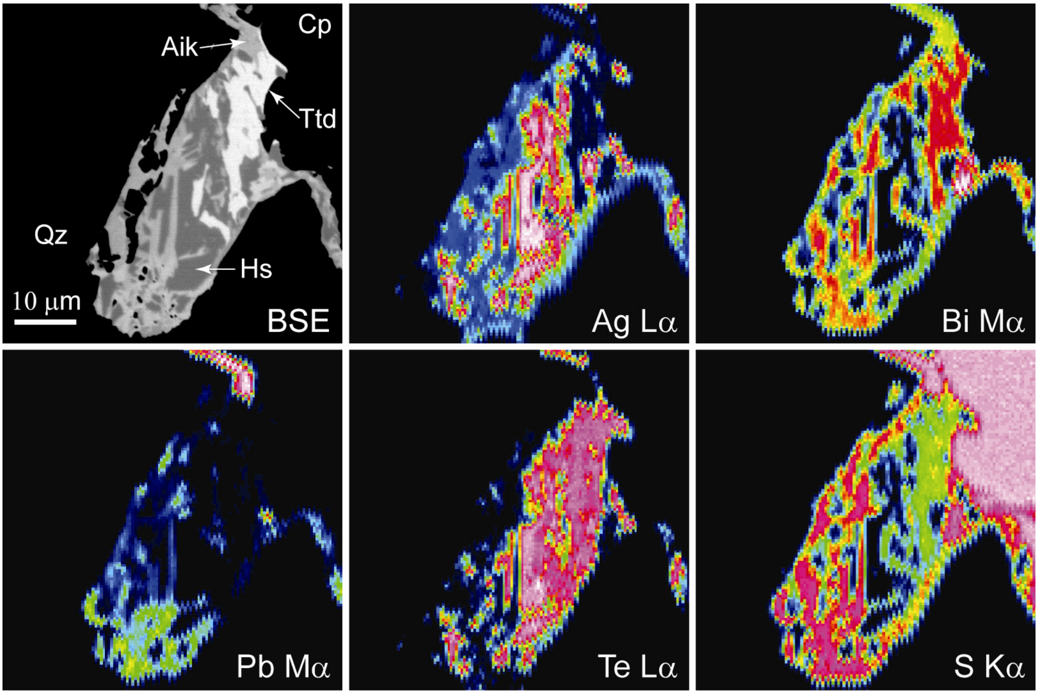

Fig. 7. X-ray elemental mapping of a complex tetradymite-hessite-aikinite intergrowth. *Abbreviations:* (Aik) aikinite; (Cp) chalcopyrite; (Hs) hessite; (Ttd) tetradymite; (Qz) quartz

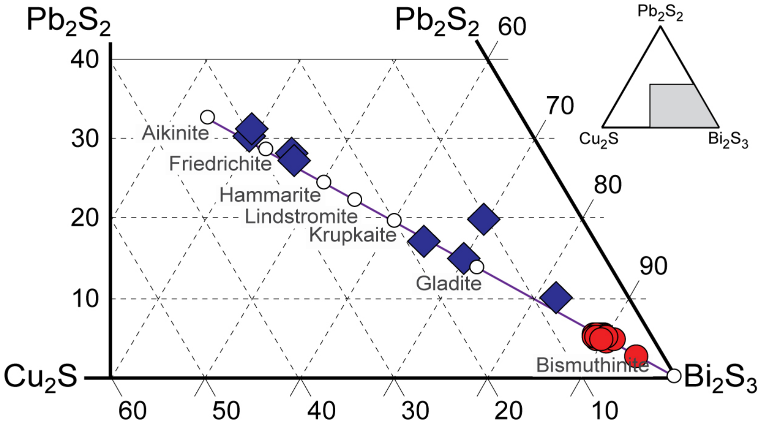

Fig. 8. Ternary Cu_2S-Bi_2S_3-Pb_2S_2 plot indicating compositions of aikinite-bismuthinite series minerals. In red – bismuthinite from type-1 and type-3 mineralization; in blue – compositions from the tetradymite-hessite-aikinite intergrowth from type-2 mineralization. Theoretical compositions are according to Makovicky & Makovicky (1978)

Table 2. *Electron microprobe analyses of bismuthinite*

	Analysis (wt. %)									Calculated formula
Label	Fe	Cu	Ag	Sb	Pb	Bi	S	Se	Te	Total	(on the basis of 5 *apfu*)*
AN-11_A	n.d.	0.68	n.d.	0.22	2.01	77.00	20.20	n.d.	n.d.	100.11	$(Bi_{1.81}Pb_{0.05}Cu_{0.05}Sb_{0.01})_{1.92}S_{3.08}$
AN-11_A	n.d.	0.66	n.d.	0.30	2.02	77.53	18.43	0.09	n.d.	99.03	$(Bi_{1.92}Pb_{0.05}Cu_{0.05}Sb_{0.01})_{2.03}S_{2.97}$
AN-11_A	0.25	0.67	n.d.	0.24	2.11	78.13	18.55	0.09	n.d.	100.04	$(Bi_{1.92}Pb_{0.05}Cu_{0.05}Sb_{0.01})_{2.03}S_{2.97}$
AN-11_C	n.d.	1.29	n.d.	0.46	3.97	75.75	18.26	0.07	n.d.	99.80	$(Bi_{1.86}Pb_{0.10}Cu_{0.10}Sb_{0.02})_{2.08}S_{2.92}$
AN-11_C	n.d.	1.25	n.d.	0.54	3.81	74.82	19.08	n.d.	n.d.	99.51	$(Bi_{1.80}Pb_{0.09}Cu_{0.10}Sb_{0.02})_{2.01}S_{2.99}$
AN-11_C	n.d.	1.27	n.d.	0.54	4.08	75.36	18.35	n.d.	n.d.	99.59	$(Bi_{1.85}Pb_{0.10}Cu_{0.10}Sb_{0.02})_{2.07}S_{2.93}$
AN-11_C	n.d.	1.17	n.d.	0.35	4.09	74.70	18.89	0.08	n.d.	99.27	$(Bi_{1.81}Pb_{0.10}Cu_{0.09}Sb_{0.01})_{2.01}S_{2.99}$
AN-11_C	0.08	1.44	n.d.	0.47	3.82	75.57	18.11	0.08	n.d.	99.56	$(Bi_{1.86}Pb_{0.09}Cu_{0.12}Sb_{0.02})_{2.09}S_{2.91}$
AN-11_B	0.43	1.19	n.d.	0.45	4.38	74.96	18.71	0.05	n.d.	100.16	$(Bi_{1.82}Pb_{0.11}Cu_{0.09}Sb_{0.02})_{2.04}S_{2.96}$
AN-11_B	0.58	1.13	n.d.	0.44	3.83	75.55	18.10	0.08	n.d.	99.71	$(Bi_{1.87}Pb_{0.10}Cu_{0.09}Sb_{0.02})_{2.08}S_{2.92}$
AN-11_D	n.d.	1.16	n.d.	0.60	4.18	75.30	18.40	0.09	n.d.	99.73	$(Bi_{1.84}Pb_{0.10}Cu_{0.09}Sb_{0.03})_{2.06}S_{2.94}$
AN-11_D	n.d.	1.30	n.d.	0.44	3.90	74.87	18.79	n.d.	n.d.	99.29	$(Bi_{1.81}Pb_{0.10}Cu_{0.10}Sb_{0.02})_{2.03}S_{2.97}$
AN-11_F	n.d.	1.35	n.d.	0.52	4.32	74.52	18.39	0.06	n.d.	99.16	$(Bi_{1.83}Pb_{0.11}Cu_{0.11}Sb_{0.02})_{2.07}S_{2.93}$
AN-11_F	n.d.	1.27	n.d.	0.40	3.97	75.08	18.78	n.d.	n.d.	99.50	$(Bi_{1.82}Pb_{0.10}Cu_{0.10}Sb_{0.02})_{2.04}S_{2.96}$
AN-11_L	n.d.	1.35	n.d.	0.29	4.12	75.55	18.25	0.06	n.d.	99.62	$(Bi_{1.86}Pb_{0.10}Cu_{0.11}Sb_{0.01})_{2.08}S_{2.92}$
AN-11_L	n.d.	1.42	n.d.	0.46	4.28	74.33	18.63	n.d.	n.d.	99.12	$(Bi_{1.81}Pb_{0.11}Cu_{0.11}Sb_{0.02})_{2.05}S_{2.95}$
AN-40-1_C1	0.15	1.31	n.d.	0.54	3.98	74.63	18.46	0.10	n.d.	99.17	$(Bi_{1.83}Pb_{0.10}Cu_{0.11}Sb_{0.02})_{2.06}S_{2.94}$
AN-40-1_C2	0.18	1.41	n.d.	0.42	4.28	75.02	18.04	n.d.	n.d.	99.35	$(Bi_{1.85}Pb_{0.11}Cu_{0.11}Sb_{0.02})_{2.09}S_{2.91}$
AN-40-1_B	n.d.	1.30	n.d.	0.46	4.37	74.13	18.46	0.06	n.d.	98.77	$(Bi_{1.82}Pb_{0.11}Cu_{0.10}Sb_{0.02})_{2.05}S_{2.95}$
AN-40-1_B	n.d.	1.38	n.d.	0.48	4.52	75.13	18.09	n.d.	n.d.	99.60	$(Bi_{1.85}Pb_{0.11}Cu_{0.11}Sb_{0.02})_{2.09}S_{2.91}$
AN-40-1_A	n.d.	1.28	n.d.	0.43	4.32	75.11	18.16	0.06	n.d.	99.36	$(Bi_{1.85}Pb_{0.11}Cu_{0.10}Sb_{0.02})_{2.08}S_{2.92}$
AN-40-1_A	0.07	1.46	n.d.	0.45	4.25	74.49	18.37	0.05	n.d.	99.14	$(Bi_{1.82}Pb_{0.10}Cu_{0.12}Sb_{0.02})_{2.06}S_{2.94}$

Table 2. (Continuation)

Label	Analysis (wt. %) Fe	Cu	Ag	Sb	Pb	Bi	S	Se	Te	Total	Calculated formula (on the basis of 5 *apfu*)*
AN-11_1	n.d.	1.37	0.07	0.53	3.94	75.93	18.49	0.07	0.13	100.54	$(Bi_{1.84}Pb_{0.10}Cu_{0.11}Sb_{0.02})_{2.07}S_{2.93}$
AN-11_2	n.d.	1.41	n.d.	0.40	3.88	75.31	18.52	0.08	0.07	99.67	$(Bi_{1.83}Pb_{0.10}Cu_{0.11}Sb_{0.02})_{2.06}S_{2.94}$
AN-11_3	0.08	1.55	n.d.	0.49	4.40	76.16	18.60	0.06	0.14	101.47	$(Bi_{1.83}Pb_{0.11}Cu_{0.12}Sb_{0.02})_{2.08}S_{2.92}$
AN-11_4	n.d.	1.38	0.09	0.53	4.06	76.27	18.48	0.09	n.d.	100.91	$(Bi_{1.85}Pb_{0.10}Cu_{0.11}Sb_{0.02})_{2.08}S_{2.92}$
AN-11_5	n.d.	1.30	0.08	0.36	4.50	75.57	18.39	0.11	0.07	100.37	$(Bi_{1.84}Pb_{0.11}Cu_{0.10}Sb_{0.01})_{2.06}S_{2.94}$
AN-11_8	n.d.	1.42	0.07	0.51	3.82	75.86	18.48	0.08	0.06	100.32	$(Bi_{1.84}Pb_{0.09}Cu_{0.11}Sb_{0.02})_{2.06}S_{2.94}$
AN-11_9	0.05	1.50	0.13	0.48	4.03	75.63	18.23	0.10	0.14	100.28	$(Bi_{1.85}Pb_{0.10}Cu_{0.12}Sb_{0.02})_{2.09}S_{2.91}$
AN-11_10	n.d.	1.53	0.09	0.50	4.22	75.76	18.78	0.11	0.12	101.12	$(Bi_{1.82}Pb_{0.10}Cu_{0.12}Sb_{0.02})_{2.06}S_{2.94}$
AN-11_11	n.d.	1.44	n.d.	0.45	4.35	75.83	18.20	0.07	0.11	100.46	$(Bi_{1.86}Pb_{0.11}Cu_{0.12}Sb_{0.02})_{2.11}S_{2.89}$
AN-11_12	n.d.	1.51	n.d.	0.42	4.21	76.31	18.37	0.09	n.d.	100.90	$(Bi_{1.85}Pb_{0.10}Cu_{0.12}Sb_{0.02})_{2.09}S_{2.91}$
AN-11_13	n.d.	1.37	n.d.	0.52	4.19	76.12	18.45	n.d.	0.07	100.72	$(Bi_{1.85}Pb_{0.10}Cu_{0.11}Sb_{0.02})_{2.08}S_{2.92}$
AN-11_16	0.30	1.24	n.d.	0.37	3.67	76.57	17.90	n.d.	n.d.	100.05	$(Bi_{1.90}Pb_{0.09}Cu_{0.10}Sb_{0.02})_{2.11}S_{2.89}$
AN-11_17	0.43	0.99	0.07	0.43	3.96	76.48	18.61	0.10	0.10	101.17	$(Bi_{1.90}Pb_{0.09}Cu_{0.10}Sb_{0.02})_{2.11}S_{2.89}$
AN-60_2	0.08	1.45	n.d.	0.52	4.21	75.64	18.55	n.d.	n.d.	100.43	$(Bi_{1.83}Pb_{0.10}Cu_{0.12}Sb_{0.02})_{2.07}S_{2.93}$
AN-60_2	0.09	1.42	n.d.	0.51	4.16	75.00	18.61	0.08	0.08	99.95	$(Bi_{1.82}Pb_{0.10}Cu_{0.11}Sb_{0.02})_{2.05}S_{2.95}$
AN-60_2	0.00	1.14	n.d.	0.54	4.19	76.14	18.51	0.11	0.11	100.73	$(Bi_{1.85}Pb_{0.10}Cu_{0.09}Sb_{0.02})_{2.06}S_{2.94}$
AN-60_2	0.11	1.35	n.d.	0.52	4.02	76.06	18.47	0.09	0.10	100.74	$(Bi_{1.85}Pb_{0.10}Cu_{0.11}Sb_{0.02})_{2.08}S_{2.92}$
AN-60_2	0.06	1.36	n.d.	0.54	3.97	75.79	18.76	0.05	n.d.	100.51	$(Bi_{1.83}Pb_{0.10}Cu_{0.11}Sb_{0.02})_{2.06}S_{2.94}$
Mean (n = 40)	0.18	1.29	0.09	0.45	3.96	75.60	18.50	0.08	0.10	100.24	$(Bi_{1.84}Pb_{0.10}Cu_{0.10}Sb_{0.01})_{2.05}S_{2.95}$
St. dev.	0.16	0.21	0.02	0.09	0.58	0.83	0.37	0.02	0.03		

n.d. - below limit of detection; LOD - Fe (0.07), Ag (0.04), Se (0.04), Te (0.05)
* formula calculation excludes minor Fe, Ag, Se and Te

Table 3. *Electron microprobe analyses of tetradymite, hessite and aikinite*

		Analysis (wt. %)									Calculated formula
No	Label	Fe	Cu	Ag	Pb	Bi	S	Se	Te	Total	
Tetradymite as single inclusions in chalcopyrite											(on the basis of 5 *apfu*)*
1	AN-35A_A	1.19	1.77	0.12	10.48	50.63	4.82	1.07	29.74	99.81	$(Bi_{1.64}Pb_{0.34}Fe_{0.14}Cu_{0.19}Ag_{0.01})_{2.32}(S_{1.02}Se_{0.09}Te_{1.57})_{2.68}$
2	AN-35A_A	0.76	1.22	17.05	6.61	39.27	3.99	0.82	30.35	100.06	$(Bi_{1.20}Pb_{0.20}Fe_{0.09}Cu_{0.12}Ag_{1.01})_{2.62}(S_{1.02}Se_{0.09}Te_{1.57})_{2.38}$
3	AN-35A_A	1.25	1.77	0.06	9.07	51.54	4.83	1.14	31.35	101.01	$(Bi_{1.64}Pb_{0.29}Fe_{0.15}Cu_{0.19})_{2.25}(S_{1.00}Se_{0.10}Te_{1.63})_{2.73}$
4	AN-35A_A	0.74	1.17	0.60	11.54	49.54	4.94	1.09	30.22	99.82	$(Bi_{1.61}Pb_{0.38}Fe_{0.09}Cu_{0.12}Ag_{0.04})_{2.25}(S_{1.05}Se_{0.09}Te_{1.71})_{2.75}$
5	AN-35A_A	0.46	0.84	0.07	9.18	50.54	4.74	1.03	31.03	97.89	$(Bi_{1.70}Pb_{0.31}Fe_{0.06}Cu_{0.09)2.16}(S_{1.04}Se_{0.09}Te_{1.71})_{2.84}$
6	AN-35A_B	0.50	0.90	0.13	7.73	52.86	4.56	1.23	31.38	99.29	$(Bi_{1.76}Pb_{0.26}Fe_{0.06}Cu_{0.10}Ag_{0.01})_{2.19}(S_{0.99}Se_{0.11}Te_{1.71})_{2.81}$
7	AN-35A_B	0.42	0.91	0.09	7.14	52.51	4.67	1.32	32.03	99.08	$(Bi_{1.74}Pb_{0.24}Fe_{0.05}Cu_{0.10}Ag_{0.01})_{2.14}(S_{1.01}Se_{0.12}Te_{1.74})_{2.86}$
8	AN-35A_F	0.11	0.30	0.06	6.65	53.70	4.52	1.08	32.47	98.88	$(Bi_{1.82}Pb_{0.23}Fe_{0.01}Cu_{0.03})_{2.10}(S_{1.00}Se_{0.10}Te_{1.80})_{2.90}$
9	AN-35A_F	0.21	0.40	0.09	7.84	52.83	4.69	1.06	32.71	99.84	$(Bi_{1.76}Pb_{0.26}Fe_{0.03}Cu_{0.04}Ag_{0.01})_{2.10}(S_{1.02}Se_{0.09}Te_{1.79})_{2.90}$
10	AN-35A_1	0.35	0.57	0.09	7.59	54.96	4.42	0.95	32.16	101.08	$(Bi_{1.83}Pb_{0.26}Fe_{0.04}Cu_{0.06}Ag_{0.01})_{2.20}(S_{0.96}Se_{0.08}Te_{1.76})_{2.80}$
11	AN-35A_2	0.49	0.84	0.11	8.97	53.49	4.64	0.97	32.43	101.94	$(Bi_{1.75}Pb_{0.30}Fe_{0.06}Cu_{0.09}Ag_{0.01})_{2.20}(S_{0.99}Se_{0.08}Te_{1.73})_{2.80}$
12	AN-35A_3	0.46	0.84	0.06	8.54	53.72	4.42	0.98	32.27	101.30	$(Bi_{1.78}Pb_{0.28}Fe_{0.06}Cu_{0.09})_{2.21}(S_{0.95}Se_{0.09}Te_{1.75})_{2.79}$
13	AN-35A_4	0.46	0.87	0.09	10.20	52.73	4.67	1.03	32.36	102.39	$(Bi_{1.71}Pb_{0.33}Fe_{0.06}Cu_{0.09}Ag_{0.01})_{2.20}(S_{0.99}Se_{0.09}Te_{1.72})_{2.80}$
14	AN-35A_5	0.52	0.81	0.13	9.47	52.27	4.75	1.05	31.59	100.59	$(Bi_{1.72}Pb_{0.31}Fe_{0.06}Cu_{0.09}Ag_{0.01})_{2.19}(S_{1.02}Se_{0.09}Te_{1.70})_{2.81}$
15	AN-35A_6	0.52	0.81	0.11	9.35	53.16	4.70	0.94	32.15	101.74	$(Bi_{1.74}Pb_{0.31}Fe_{0.06}Cu_{0.09}Ag_{0.01})_{2.20}(S_{1.00}Se_{0.08}Te_{1.72})_{2.80}$
	Mean (n=15)	0.56	0.93	1.26	8.69	51.58	4.62	1.05	31.61	100.32	$(Bi_{1.69}Pb_{0.29}Fe_{0.07}Cu_{0.10}Ag_{0.07})_{2.22}(S_{0.99}Se_{0.09}Te_{1.70})_{2.78}$
	St. dev.	0.32	0.42	4.37	1.44	3.69	0.23	0.12	0.92		
Tetradymite intergrown with aikinite and hessite											(on the basis of 5 *apfu*)*
1	AN-35A_7	0.42	0.43	0.84	0.59	58.84	4.02	1.02	34.34	100.52	$(Bi_{1.97}Pb_{0.02}Fe_{0.05}Cu_{0.05}Ag_{0.05})_{2.15}(S_{1.02}Se_{0.09}Te_{1.57})_{2.85}$
2	AN-35A_8	0.62	0.45	1.73	0.69	56.72	4.17	1.07	34.18	99.63	$(Bi_{1.88}Pb_{0.02}Fe_{0.08}Cu_{0.05}Ag_{0.11})_{2.14}(S_{0.91}Se_{0.09}Te_{1.86})_{2.86}$
3	AN-35A_9	0.61	0.97	5.41	0.62	58.98	4.12	1.19	28.98	100.89	$(Bi_{1.93}Pb_{0.02}Fe_{0.07}Cu_{0.10}Ag_{0.34})_{2.47}(S_{0.88}Se_{0.10}Te_{1.55})_{2.53}$
4	AN-35A_10	0.31	0.25	0.84	0.64	59.29	4.46	1.02	33.79	100.59	$(Bi_{1.97}Pb_{0.02}Fe_{0.04}Cu_{0.03}Ag_{0.05})_{2.11}(S_{0.96}Se_{0.09}Te_{1.84})_{2.89}$
5	AN-35A_14	0.93	1.50	0.42	0.18	58.11	3.83	1.01	34.54	100.51	$(Bi_{1.92}Pb_{0.01}Fe_{0.11}Cu_{0.16}Ag_{0.03})_{2.23}(S_{0.82}Se_{0.09}Te_{1.86})_{2.77}$
6	AN-35A_C	0.37	0.75	1.16	1.44	56.52	4.88	1.16	31.23	97.51	$(Bi_{1.88}Pb_{0.05}Fe_{0.05}Cu_{0.08}Ag_{0.08})_{2.13}(S_{1.06}Se_{0.10}Te_{1.70})_{2.87}$
7	AN-35A_C	0.23	0.17	0.36	0.21	57.89	4.38	1.17	33.31	97.72	$(Bi_{1.98}Pb_{0.01}Fe_{0.03}Cu_{0.02}Ag_{0.02})_{2.06}(S_{0.97}Se_{0.11}Te_{1.86})_{2.94}$
8	AN-35A_C	0.34	0.13	0.61	1.12	56.24	4.34	1.35	33.32	97.45	$(Bi_{1.92}Pb_{0.04}Fe_{0.04}Cu_{0.01}Ag_{0.04})_{2.05}(S_{0.96}Se_{0.12}Te_{1.86})_{2.95}$

Table 3. (Continuation)

		Analysis (wt. %)									Calculated formula				
No	Label	Fe	Cu	Ag	Pb	Bi	S	Se	Te	Total					
9	AN-35A_E	0.18	0.46	0.20	0.43	58.03	4.61	0.94	33.53	98.39	$(Bi_{1.95}Pb_{0.01}Fe_{0.02}Cu_{0.05}Ag_{0.01})_{2.06}(S_{1.01}Se_{0.08}Te_{1.85})_{2.94}$				
10	AN-35A_H	0.10	0.22	1.06	1.02	57.47	5.10	0.96	31.70	97.63	$(Bi_{1.92}Pb_{0.03}Fe_{0.01}Cu_{0.02}Ag_{0.07})_{2.06}(S_{1.11}Se_{0.08}Te_{1.74})_{2.94}$				
11	AN-35A2_B	0.01	0.13	0.24	0.15	57.95	4.37	1.19	33.83	97.88	$(Bi_{1.98}Pb_{0.01}Cu_{0.01}Ag_{0.02})_{2.02}(S_{0.98}Se_{0.11}Te_{1.90})_{2.98}$				
	Mean (n=11)	0.37	0.50	1.17	0.65	57.82	4.39	1.10	32.98	98.97	$(Bi_{1.94}Pb_{0.02}Fe_{0.05}Cu_{0.05}Ag_{0.08})_{2.14}(S_{0.96}Se_{0.10}Te_{1.81})_{2.87}$				
	St. dev.	0.26	0.43	1.48	0.41	1.01	0.37	0.13	1.68						
Hessite intergrown with tetradymite and aikinite											(on the basis of 3 *apfu*)*				
1	AN-35A_12	0.12	0.03	62.76	0.27	0.16	0.16	0.08	37.21	100.77	$(Ag_{1.98}Fe_{0.01})_{1.99}(Te_{0.99}S_{0.02})_{1.01}$				
2	AN-35A_13	0.52	0.08	62.03	0.09	0.67	0.14	n.d.	36.76	100.29	$(Ag_{1.97}Fe_{0.03})_{2.00}(Te_{0.98}S_{0.02})_{1.00}$				
3	AN-35A_15	0.13	0.40	62.73	n.d.	0.12	0.10	0.07	37.24	100.79	$(Ag_{1.97}Fe_{0.01}Cu_{0.02})_{2.00}(Te_{0.99}S_{0.01})_{1.00}$				
4	AN-35A_C	0.39	1.03	61.64	0.22	0.47	0.98	0.08	33.24	98.06	$(Ag_{1.94}Fe_{0.02}Cu_{0.05})_{2.01}(Te_{0.88}S_{0.11})_{0.99}$				
5	AN-35A_C	0.46	0.97	61.49	n.d.	0.15	0.82	n.d.	34.44	98.33	$(Ag_{1.92}Fe_{0.03}Cu_{0.05})_{2.00}(Te_{0.91}S_{0.09})_{1.00}$				
6	AN-35A_C	0.33	0.49	62.13	0.11	0.28	0.52	n.d.	35.08	98.93	$(Ag_{1.96}Fe_{0.02}Cu_{0.03})_{2.01}(Te_{0.94}S_{0.05})_{0.99}$				
7	AN-35A_C	0.17	0.51	61.18	0.09	0.47	0.43	n.d.	35.09	97.94	$(Ag_{1.96}Fe_{0.01}Cu_{0.03})_{2.00}(Te_{0.95}S_{0.05})_{1.00}$				
8	AN-35A_H	0.09	0.30	60.92	0.06	0.20	0.29	0.05	35.88	97.79	$(Ag_{1.97}Fe_{0.01}Cu_{0.02})_{2.00}(Te_{0.98}S_{0.02})_{1.00}$				
9	AN-35A2_B	0.08	0.43	62.30	n.d.	0.15	0.40	n.d.	35.59	98.95	$(Ag_{1.98}Cu_{0.02})_{2.00}(Te_{0.96}S_{0.04})_{1.00}$				
	Mean (n=9)	0.25	0.47	61.91	0.14	0.30	0.43	0.07	35.61	99.18	$(Ag_{1.95}Fe_{0.02}Cu_{0.03})_{2.00}(Te_{0.95}S_{0.05})_{1.00}$				
	St. dev.	0.17	0.34	0.65	0.09	0.20	0.31	0.01	1.33						
											Cat %				
Aikinite-bismuthinite ss intergrown with tetradymite and hessite											Fe	Cu	Ag	Pb	Bi
1	AN-35A_C	0.49	9.41	0.38	30.97	40.60	17.17	0.53	0.19	99.74	1.73	29.38	0.71	29.65	38.54
2	AN-35A_C	0.19	7.43	7.61	25.47	41.13	14.41	0.73	3.85	100.82	0.67	22.91	13.82	24.06	38.54
3	AN-35A_C	0.21	8.07	0.73	26.81	45.22	17.19	0.68	0.49	99.39	0.80	26.27	1.39	26.77	44.78
4	AN-35A_E	0.19	3.43	11.57	11.24	53.15	17.16	1.44	1.06	99.25	0.72	11.41	22.67	11.46	53.74
5	AN-35A_E	0.26	2.35	11.45	14.64	52.20	17.17	1.50	1.11	100.68	1.01	7.89	22.67	15.09	53.34
6	AN-35A_H	0.35	1.62	12.79	6.88	58.75	17.52	1.01	0.77	99.69	1.37	5.47	25.52	7.15	60.49
7	AN-35A_J	0.16	4.27	11.83	13.28	50.76	17.42	1.12	0.93	99.76	0.57	13.80	22.54	13.17	49.91
8	AN-35A2_B	0.04	9.15	n.d.	31.81	40.37	17.37	0.47	0.06	99.27	0.14	29.30	0.05	31.22	39.29

contamination from the host chalcopyrite during the microprobe analyses.

The compositions of *aikinite-bismuthinite derivates,* occurring as part of the complex intergrowth with hessite and tetradymite in type-II mineralization, plot along the aikinite-bismuthinite series on the Cu_2S-Bi_2S_3-Pb_2S_2 diagram (Fig. 8). The analytical points indicate aikinite-friedrichite, friedrichite-hammarite, krupkaite-gladite, and gladite-bismuthinite intermediate compositions, according to the compositional fields defined by Makovicky & Makovicky (1978) and Mozgova et al. (1990). Lead concentrations are often different even within a single intergrowth texture, as revealed by X-ray elemental mapping (Fig. 7) and correlates with Bi, indicating Pb-Bi substitution. Microprobe analyses (Table 3) systematically show very high concentrations of Ag (up to 12.79 wt.%) which most probably is due to the presence of submicroscopic Ag-bearing phase, rather than to contamination from the neighboring hessite. The small size of the analyzed crystals was the major limiting factor during the microprobe sessions. However, positive 1:1 correlation between Cu and Pb (Fig. 9c) and negative 1:1 correlation between Cu and Bi (Fig. 9d) is registered for the studied minerals, as it is expected from the general substitution scheme $Cu^+ + Pb^{2+} \leftrightarrow \square + Bi^{3+}$ in the aikinite-bismuthinite series (Makovicky & Makovicky 1978).

Hessite (Ag_2Te) is often the dominant phase in the complex intergrowth textures (Fig. 6e-f). The mineral always contains minor amount of Fe, Cu, Pb, Bi, S and Se, usually <1 wt.% (Table 3). The observed strong Te – (S+Se) correlation (Fig. 9e) suggests the following substitution mechanism in the anions $S^{2-} + Se^{2-} \leftrightarrow 2Te^{2-}$. No correlation between the other trace elements has been observed.

Discussion

Mineralogy of the Cu-Bi-Pb-Ag-Te assemblage

The mineralization described in the different types of samples from the central part of the Modi-Khola valley has very similar Cu-Bi-Pb-Ag-Te geochemical signature, which is the main argument to relate them to one and the same hydrothermal system. The main difference between the two types of analyzed samples comes from the Bi-bearing minerals in the paragenesis. Bismuthinite is the only Bi-bearing phase in type-I and III mineralization, while in type-II bismuthinite is absent and complex tetradymite-hessite-aikinite intergrowths occur instead. Despite the common presence of Cu and Pb in the bismuthinite, breakdown of a phase with similar composition could not explain the formation of the tetradymite-hessite-aikinite intergrowth textures. Silver was detected as a very minor component of bismuthinite, further lowering the chance of Ag-bearing phases to have formed by exsolution. In addition, highly variable phase proportions between the three minerals in the textures also favor a simple intergrowth mechanism of formation. Thus, the two textural types of ore most probably belong to the same mineralization system, but represent spatial variations.

Similar to the studied complex intergrowth textures, involving Bi-, Pb-, and Ag-bearing sulphides, sulphosalts and tellurides have been described in different geological contexts – in polymetallic mesothermal veins of the Bakadjik deposit, Bulgaria (Breskovska et al. 1984); veins in carbonate-hosted high-temperature polymetallic replacement bodies of the Ardino deposit, south Bulgaria (Bonev & Neykov 1990); in the stringer zones of

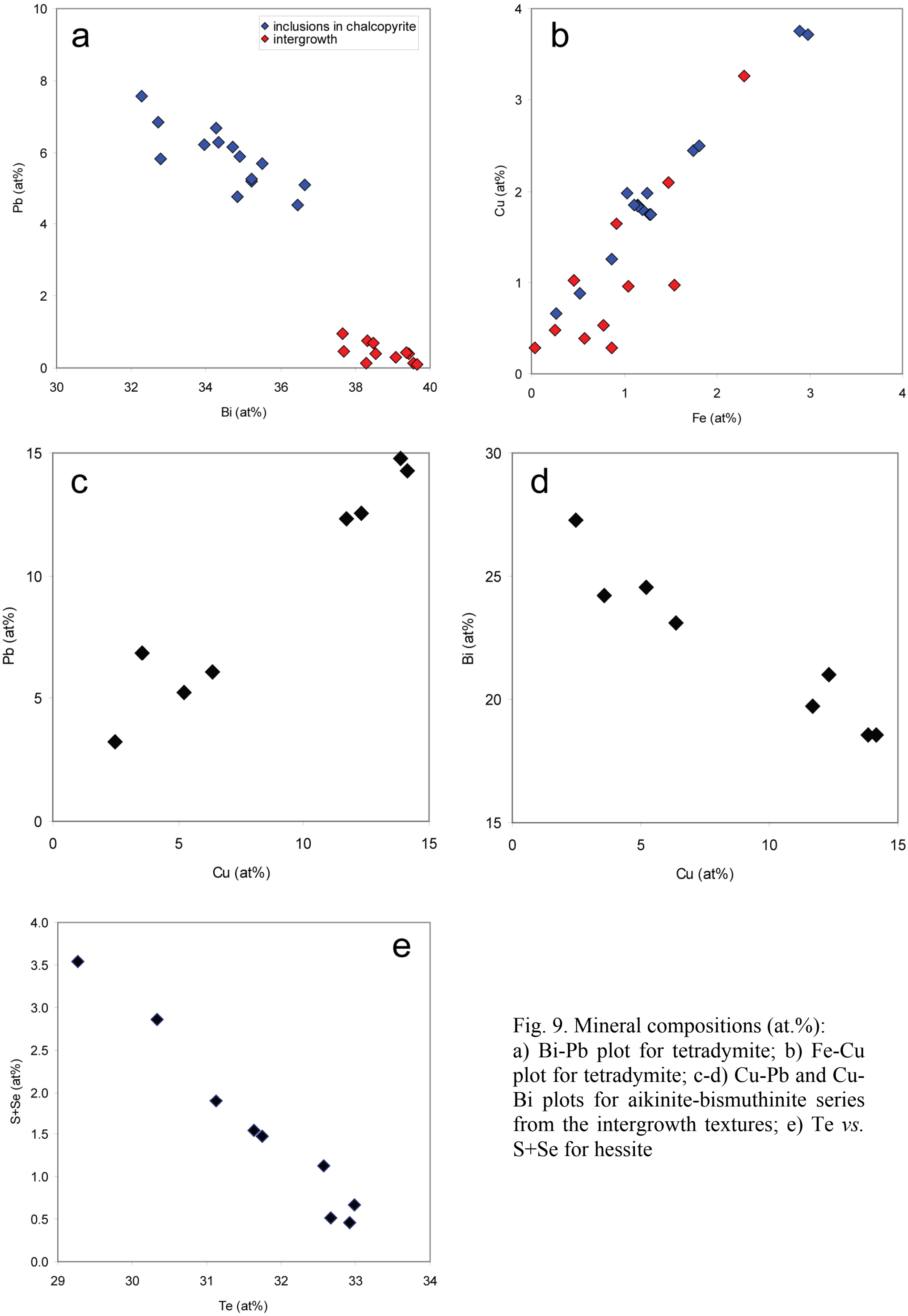

Fig. 9. Mineral compositions (at.%): a) Bi-Pb plot for tetradymite; b) Fe-Cu plot for tetradymite; c-d) Cu-Pb and Cu-Bi plots for aikinite-bismuthinite series from the intergrowth textures; e) Te *vs.* S+Se for hessite

volcanogenic massive sulphide deposits of the Iberian Pyrite Belt (Marcoux et al. 1996); in polymetallic veins of the Larga hydrothermal system, Metaliferi Mountains, Romania (Cook & Ciobanu 2004). In most of the deposits cited above fluid inclusion microthermometry and/or mineral stabilities indicate mesothermal conditions of ore formation, typically in the interval 450-350°C. In such conditions as suggested by Cook & Ciobanu (2004) Ag- and Bi-tellurides were extracted from fluids as Ag-Bi-Te-(S) "melts" at temperatures above the melting point of bismuth (271°C), and formed equilibrium assemblages with the bulk composition of the initial "droplet". In addition, the speciation of Bi-tellurides, with Bi/Te(+Se+S)≤1 (tetradymite) is consistent with a pyrite-buffered environment.

Possible genesis of the studied mineralization

We can assume mesothermal conditions of ore formation for the studied moraine-hosted Cu-Bi mineralization from the southwestern flank of Annapurna-III, based as well on the mineral paragenesis: high-temperature minerals such as ilmenite, magnetite, garnet, rutile, and cubanite are constantly present. Because of the small size of the quartz crystals associated with this mineralization, fluid inclusion microthermometry was not possible to be applied in order to estimate the *P-T* conditions of formation. The lack of any data on the hydrothermal alteration associated with the mineralization makes also difficult the genetical interpretation. However, taking into account the nature of the host rock (hydrothermal breccia, crosscutting strongly silicified marble and veinlets and dissemination affecting leucocratic magmatic rock) two possible scenarios can be proposed, both related to a magma-derived hydrothermal system. The mineralization can be genetically related to leucogranite intrusions, emplaced along the South Tibetan detachment fault (Fig. 1) and affecting the marbles of the footwall of the structure (Fig. 2). The Manaslu granites (Guillot et al. 1995) intruding the STD plane in the studied area are the most probable source of the fluids. To the east of the Annapurna range, in the Tibetan plateau, leucogranite intrusions are also genetically related to porphyry Cu-Mo and Cu-Au systems of Miocene age (Hou et al. 2004; 2009). The equigranular pegmatite bodies, which are abundant in the area and crosscut the sequence of Unit-II (Fig. 2), can be regarded as a second potential source of magmatic fluids. Supporting the second hypothesis, Vassileva & Bonev (2008) described highly oxidized (over pyrite) pegmatite bodies in the middle part of the Modi-Khola valley, suggesting hydrothermal activity related to the emplacement of the latter.

Conclusions

The mineralogical and geochemical Cu-Bi-Ag-Te signature of the breccia-hosted and disseminated mineralization found in loose boulders of silicified marbles and leucocratic magmatites in the central part of the Modi-Khola valley, on the southern flank of the Annapurna-III, suggest dominantly magmatic source for the mineralizing fluids. As suggested by Craw (1990) the thermal anomaly in the Annapurna Himal associated with rapid Himalayan uplift along the MCT and with the emplacement of orogenic granites along the STD, was a Miocene feature and is not related to the present day warm springs which are abundant in the Annapurna range.

For the first time high-temperature hydrothermal mineralization is described in the studied area. The mineralogical and geochemical features of this formation allow us to define it as a new type of ore-forming system in the post-collisional metallogenic context of the high Himalaya. Hou & Cook (2009) defined in the Tibetan orogen another vein type Sb-Au ore system in a similar structural position – controlled by the STD and the metamorphic core complex or thermal dome intruded by leucogranite intrusions. To unravel the real genesis of this mineralization, stable isotope and fluid inclusions studies are needed.

References

Allègre CJ, Courtillot V, Tapponnier P, Hirn A, Mattauer M, Coulon C, Jaeger JJ, Achache J, Scharer U, Marcoux J, Burg JP, Girardeau J, Armijo R, Gariepy C, Gopel C, Li T, Xiao XC, Chang CF (1984) Structure and evolution of the Himalaya–Tibet orogenic belt. *Nature*, **307**, 17-22.

Bonev IK, Neykov HN (1990) Minerals of silver, bismuth and tellurium in Ardino polymetallic deposit. *Geochemistry, Mineralogy and Petrology*, **26**, 3-19.

Bordet P, Colhen M, Krummenacher D, Le Fort P, Mouterde R, Remy M (1971) Recherche géologiques dans l'Himalaya du Népal: région de la Thakkhola. CNRS, Paris, 279 p.

Breskovska VV, Mozgova NN, Bortnikov NS, Tzepin AI, Borodaev YS (1984) New data on the bismuth sulphosalts from the Bakagjik polymetallic deposit, Yambol district, Bulgaria. *Annuaire de l'Universite de Sofia «St. Kliment Ohridski»*, **78**, 182-191.

Colchen M, Le Fort P, Pêcher A (1986) *Annapurna-Manaslu-Ganesh Himal*. CNRS, Paris, p 136.

Cook NJ, Ciobanu CL (2004) Bismuth tellurides and sulphosalts from the Larga hydrothermal system, Metaliferi Mts., Romania: Paragenesis and genetic significance. *Mineralogical Magazine*, **68**, 301-321.

Craw D (1990) Fluid evolution during uplift of the Annapurna Himal, central Nepal. *Lithos*, **24**, 137-150.

Dhital MR, Thapa PB, Ando H (2002) Geology of the inner Lesser Himalaya between Kusma and Syangja in western Nepal. *Bulletin of the Department of Geology, Tribhuvan University,* Kathmandu, Nepal, **9**, 1-60.

England P, Le Fort P, Molnar P, Pêcher A (1992) Heat sources for tertiary metamorphism in the Annapurna-Manaslu region, central Nepal. *Journal of Geophysical Research*, **97**, B2, 2107-2128.

Gansser A (1964) *Geology of the Himalayas*. Wiley-Interscience, London, 289 p.

Garzanti E (1999) Stratigraphy and sedimentary history of the Nepal Tethys Himalaya passive margin. *Journal of Asian Earth Sciences*, **17**, 805-827.

Godin L (2003) Structural evolution of the Thetyan sedimentary sequence in the Annapurna area, central Nepal Himalaya. *Journal of Asian Earth Sciences*, **22**, 307-328.

Godin L, Parrish RR, Brown RL, Hodges KV (2001) Crustal thickening leading to exhumation of the Himalayan metamorphic core of central Nepal: insight from U–Pb geochronology and 40Ar/39Ar thermochronology. *Tectonics*, **20**, 729-747.

Godin L, Gleeson T, Searle MP, Ullrich TD, Parrish RR (2006) Locking of southward extrusion in favour of rapid crustal-scale buckling of the Greater Himalayan sequence, Nar valley, Central Nepal. In: Law RD, Searle MP, Godin L (Editors) *Channel Flow, Ductile Extrusion and Exhumation in Continental Collision Zones*. Geological Society, London, Special Publication, **268**, 269-292.

Guillot S, Le Fort P, Pêcher A, Barman MR, Aprahamian J (1995) Contact metamorphism and depth of emplacement of the Manaslu granite (central Nepal): Implications for Himalayan orogenesis. *Tectonophysics*, **241**, 99–119.

Harrison TM, McKeegan KD, Le Fort P (1995) Detection of inherited monazite in the Manaslu leucogranite by 208Pb/ 232Th ion microprobe dating; crystallization age and tectonic implications. *Earth and Planetary Science Letters*, **133**, 271-282.

Harrison TM, Grove M, McKeegan KD, Coath CD, Lovera OM, Le Fort P (1999) Origin and episodic emplacement of the Manaslu intrusive complex, central Himalaya. *Journal of Petrology*, **40**, 3-19.

Hodges KV, Parish RR, Searle MP (1996) Tectonic evolution of the central Annapurna range, Nepalese Himalaya. *Tectonics*, **15**, 1264-1291.

Hou Z, Cook NJ (2009) Metallogenesis of the Tibetan collisional orogen: A review and introduction to the special issue. *Ore Geology Reviews*, **36**, 2-24.

Hou Z, Qu X, Wang S, Du A, Gao Y, Huang W (2004) Re-Os age for molybdenite from the Gandese porphyry copper belt on Tibetan plateau: Implication for geodynamic setting and duration of the Cu mineralization. *Science in China, Ser. D Earth Sciences*, **47**, 221-231.

Hou ZQ, Yang ZM, Qu XM, Meng XJ, Li ZQ, Beaudoin G, Rui ZY, Gao YF, Khin Z (2009) The Miocene Gangdese porphyry copper belt generated during post-collisional extension in the Tibetan Orogen. *Ore Geology Reviews*, **36**, 25-51.

Inger S, Harris N (1993) Geochemical constrains on leucogranite magmatism in the Langtang Valley, Nepal Himalaya. *Journal of Petrology*, **34**, 2, 345-368.

Le Fort P (1975) Himalayas: the collided range. Present knowledge of the continental arc. *American Journal of Science* **275-a,** 1-44.

Le Fort P (1981) Manaslu leucogranite: a collision signature of the Himalaya - a model for its genesis and emplacement, *Journal of Geophysical Research*, **86**, 545-568.

Le Fort P, Raï SM (1999) Pre-Tertiary felsic magmatism of the Nepal Himalaya: recycling of continental crust. *Journal of Asian Earth Sciences* 17, 607-628.

Makovicky E, Makovicky M (1978) Representation of compositions in the bismuthinite-aikinite series. *Canadian Mineralogist*, **16**, 405-409.

Marcoux E, Moelo Y, Leistel JM (1996) Bismuth and cobalt minerals as indicators of stringer zones to massive sulphide deposits, Iberian Pyrite Belt. *Mineralium Deposita*, **31**, 1-26.

Mozgova NN, Nenasheva SN, Chistyakova NI, Mogilevkhin SB, Sivtsov AV (1990) Compositional fields of minerals in the bismuthinite-aikinite series. *Neues Jahrbuch für Mineralogie Monatshefte*, **1**, 35-45.

Murphy MA, Yin A (2003) Structural evolution and sequence of thrusting in the Tethyan fold-thrust belt and Indus-Yalu suture zone, Southwest Tibet. *Geological Society of America Bulletin*, **115**, 1, 21-34.

Parrish RR, Hodges KV (1996) Isotopic constraints on the age and provenance of the Lesser and Greater Himalayan sequences, Nepalese Himalaya. *Geological Society of America Bulletin*, **108**, 904-911.

Pêcher A (1989) The metamorphism in the central Himalaya. *Journal of Metamorphic Geology*, **7**, 31-41.

Searle MP, Godin L (2003) The South Tibetan detachment and the Manaslu Leucogranite: a structural reinterpretation and restoration of the Annapurna-Manaslu Himalaya, Nepal. *Journal of Geology*, **111,** 5, 505-523

Seltmann R, Faragher AE (1994) Metallogeny of collisional orogens - a preface. In: Seltmann R, Kampf H, Moller P (Editors) *Metallogeny of Collisional Orogen*, Czech Geological Survey, Prague, 7-19.

Stöcklin J (1980) Geology of Nepal and its regional frame. *Journal of Geological Society of London*, **137**, 1-34.

Vassileva RD, Bonev IK (2008) Mineralogy of diopside-phlogopite marbles from the Modi-Khola valley, the Central Nepal Himalaya. *Geochemistry, Mineralogy and Petrology*, **46**, 69-84.

Yin A, Harrison TM (2000) Geologic evolution of the Himalayan-Tibetan orogen, *Annual Reviews of Earth and Planetary Science*, **28**, 211-280.

Accepted November 25, 2009